PARTIAL INTERACTION ANALYSIS WITH SHEAR-LAG EFFECTS OF COMPOSITE BRIDGES: A FINITE ELEMENT IMPLEMENTATION FOR DESIGN APPLICATIONS

Fabrizio Gara [1], Gianluca Ranzi [2] and Graziano Leoni [3,*]

[1] *Department of Architecture Construction and Structures, Universita' Politecnica delle Marche, Ancona, Italy*
[2] *School of Civil Engineering, The University of Sydney, Sydney, NSW2006, Australia*
[3] *School of Architecture and Design, University of Camerino, Ascoli Piceno, Italy*
**(Corresponding author: E-mail: graziano.leoni@unicam.it)*

ABSTRACT: This paper presents a numerical model for the analysis of composite steel-concrete beams with partial interaction to account for the deformability of the shear connection. The proposed approach is capable of capturing the structural response produced by shear-lag effects and by the time-dependent behaviour of the concrete. The versatility of the FE formulation is demonstrated for a wide range of realistic bridge arrangements, e.g. from twin-deck girders to cable-stayed bridges. The accuracy of the approach is validated against the results obtained from more refined models generated with shell elements using commercial finite element software. For each bridge typology considered, both deformations and stresses are calculated to provide greater insight into the structural performance. Particular attention is placed on the determination of the effective width to be used for design purposes and on the stress distribution induced in the concrete component, together with their variation with time due to creep and shrinkage.

Keywords: Cable stayed bridges, Composite bridge decks, Creep, Effective width, Shear-lag, Shrinkage, Steel-concrete members

1. INTRODUCTION

Steel-concrete composite decks are used in many bridge typologies. In addition to multi-span continuous beam arrangements, widely used in viaducts and flyovers, composite decks are also combined with other structural elements to achieve more articulated systems, such as arch bridges and cable stayed bridges, when longer spans are required. In the modelling of these structures it is common to use simple beam theory, according to which plane cross-sections remain plane after loading, even if such approach is not realistic as non-uniform stress distributions usually arise in the slab (shear-lag effect) reducing its effective width. These can also arise due to the application of concentrated loads, e.g. anchorage of prestressing cables or stays. When dealing with shear-lag effects international design guidelines recommend the use of the effective width method. While this approach is very efficient and useful for simple beam layouts, its fundamental assumptions are violated when applied to more articulated structural arrangements. In a design situation such structures may be analysed using refined models generated with shell or solid finite elements, in which case both model development and post-processing are very time-consuming. As required in international guidelines (e.g. Eurocode 4 [1]), a designer needs to evaluate the effective cross-section of a bridge girder to determine its resistance. Unfortunately, simple rules for the definition of the slab effective widths are available only for simple static cases. Another important aspect relates to the fact that the effective width is time-dependent when longitudinal concentrated forces are applied to the steel beam or to the concrete slab [2].

In this context, the finite element formulation adopted in this paper predicts the non-uniform distribution of stresses within the slab due to shear-lag effects, even in complex bridge arrangements, while maintaining the ease of use of standard line elements commonly used for frame analyses. The proposed technique is a powerful tool for the designer that can (i) analyse the structure without worrying about the effective width definition and (ii) perform the cross-sectional design calculations using the effective slab width determined from the appropriate static scheme and load layout.

The fundamental model was already proposed by the authors in [3], while in this paper the formulation is used to deal with a wide range of bridge arrangements and to account for time effects. Its use is proposed in combination with common truss and frame elements to enable the modelling of complex three-dimensional bridge arrangements.

The applications to realistic cases are discussed with particular emphasis to creep and shrinkage effects that have a great influence on the stress states and on the definition of the slab effective width.

2. OVERVIEW OF THE ANALYTICAL AND NUMERICAL MODELS OF THE DECK

A symmetric composite steel-concrete twin-girder bridge deck is considered (Figure 1). A local reference system $\{O; x_1, x_2, x_3\}$ is introduced by placing the plane x_1-x_2 on the symmetry plane of the cross-section in such a way that x_1 and x_2 are longitudinal and vertical axes of the deck, respectively. The origin O is located at an arbitrary location even if it may be conveniently placed at the centroid of the steel beams.

The cross-section is considered to be rigid in its own plane (x_2-x_3) and the interface shear connection is assumed to prevent separation and lateral slips between the steel beam and the slab while permitting relative longitudinal displacements between them.

The kinematic model for a deck subjected to flexural and axial actions in the plane x_1-x_2 is briefly outlined in the following to provide a better insight into the results presented in the applications.

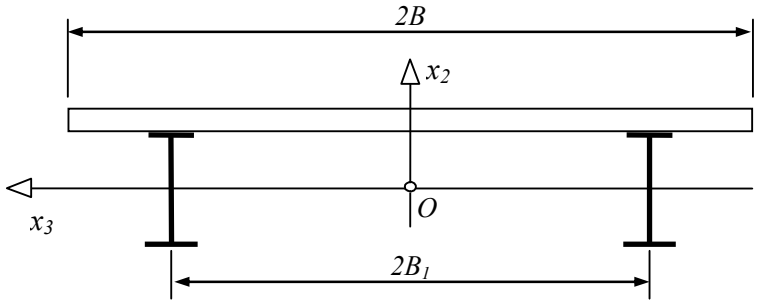

Figure 1. Steel-concrete Twin Girder Cross-section

Based on these considerations, and neglecting the shear deformability of the steel beams, the displacement of a generic point of the cross-section placed at x_1 is defined by the three components

$$d_1(x_1,x_2,x_3)=\begin{cases} u_1(x_1)-x_2u_2'(x_1) & \forall(x_2,x_3)\in A_c \\ u_1(x_1)-\Gamma(x_1)-x_2u_2'(x_1)+\psi(x_3)\omega(x_1) & \forall(x_2,x_3)\in A_a \end{cases} \tag{1a}$$

$$d_2(x_1, x_2, x_3) = u_2(x_1) \tag{1b}$$

$$d_3(x_1, x_2, x_3) = 0 \tag{1c}$$

where the prime denotes the derivative with respect to x_1, A_c and A_a are the cross-sections of the concrete slab and the steel beam, respectively, u_1 and u_2 are the longitudinal and vertical displacements of the steel beam measured at the level of the reference axis x_1, Γ is the longitudinal slip between the steel beams and the reinforced concrete slab and ψ is the function describing the warping in the slab that is modulated along the deck axis by the intensity shear-lag function ω [4, 5].

Given the particularity of the assumed deck cross-section, it is appropriate to adopt a function ψ formed by three second order parabolic branches [6]

$$\psi(x_3) = \left(\frac{x_3}{B}\right)^2 + 2\frac{x_3}{B} + \frac{B_1}{B}\left(2 - \frac{B_1}{B}\right) \qquad -B \le x_3 \le -B_1 \tag{2a}$$

$$\psi(x_3) = \left(\frac{x_3}{B}\right)^2 - \left(\frac{B_1}{B}\right)^2 \qquad -B_1 < x_3 \le +B_1 \tag{2b}$$

$$\psi(x_3) = \left(\frac{x_3}{B}\right)^2 - 2\frac{x_3}{B} + \frac{B_1}{B}\left(2 - \frac{B_1}{B}\right) \qquad +B_1 < x_3 \le +B \tag{2c}$$

that describe rigorously the warping in the case of beams subjected to pure shear given the position of the main longitudinal beams.

Under the assumption of linear-elastic behaviour for the materials forming the cross section and for the shear connection, a displacement-based finite element has been developed [7] and implemented for the modelling of composite beams with complex static schemes [3]. A local reference system is introduced for each element with the origin located at node *i* (Figure 2). If $\bar{x}_1$ is the longitudinal axis of the element, oriented from joint *i* to joint *j*, axes $\bar{x}_2$ and $\bar{x}_3$ complete an ortho-normal reference system.

The nodal displacements of the finite element are defined according to the positive directions of the local reference axes. For each node, three displacement components and three rotation components are considered. Two additional degrees of freedom are introduced to define the beam-slab interface slip Γ and the shear-lag function ω previously defined (Figure 2a). These last two generalized displacements are scalar quantities and thus do not depend on the adopted reference system.

Generalised stress resultants are defined corresponding to each of the displacements considered, i.e. three force components and three moments, the longitudinal shear force at beam slab interface and the slab bi-moment (Figure 2b). As for the displacements, the last two generalized actions are scalar quantities.

The generalized nodal displacements and forces of element *e* are grouped in the vectors

$$\boldsymbol{s_i}^T = \left[u_{1i} \quad u_{2i} \quad u_{3i} \quad \varphi_{1i} \quad \varphi_{2i} \quad \varphi_{3i} \quad \Gamma_i \quad \omega_i \;\vdots\; u_{1j} \quad u_{2j} \quad u_{3j} \quad \varphi_{1j} \quad \varphi_{2j} \quad \varphi_{3j} \quad \Gamma_j \quad \omega_j\right] \tag{3a}$$

$$\boldsymbol{f_i}^T = \left[f_{1i} \quad f_{2i} \quad f_{3i} \quad m_{1i} \quad m_{2i} \quad m_{3i} \quad q_i \quad \beta_i \;\vdots\; f_{1j} \quad f_{2j} \quad f_{3j} \quad m_{1j} \quad m_{2j} \quad m_{3j} \quad q_j \quad \beta_j\right] \tag{3b}$$

Based on the adopted material properties, the stiffness relationship of the line element can be expressed as $\bar{\boldsymbol{f}}_{\boldsymbol{e}} = \overline{\boldsymbol{K}}_e \bar{\boldsymbol{s}}_e$, where $\overline{\boldsymbol{K}}_e$ depicts its stiffness matrix. When modelling three-dimensional structural systems, this line element can be oriented freely. Adopting an ortho-normal global reference system and introducing $\boldsymbol{a}_\alpha$ and $\bar{\boldsymbol{a}}_\alpha$ (α = 1,2,3) as unit vectors of the global and local reference systems respectively, the rotation operator $\boldsymbol{R}_e$ can be expressed using the following matrices

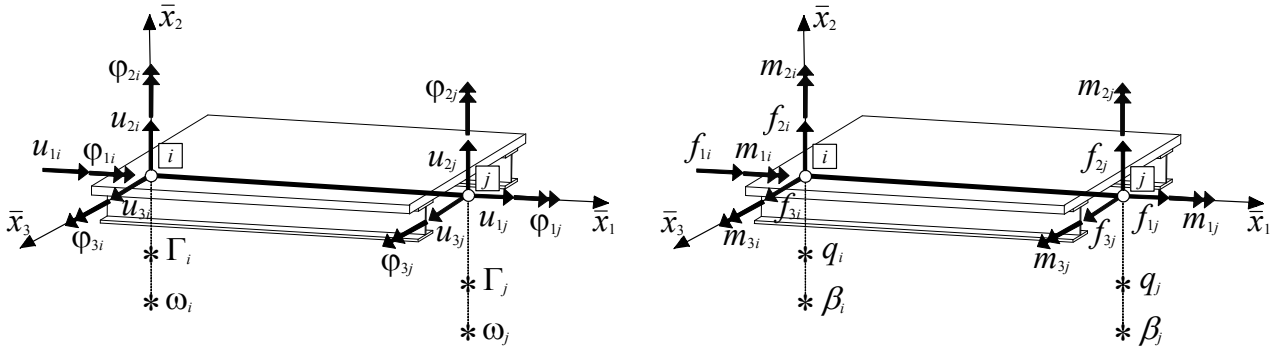

Figure 2. Composite Line Element: (a) Nodal Displacements; (b) Nodal Forces

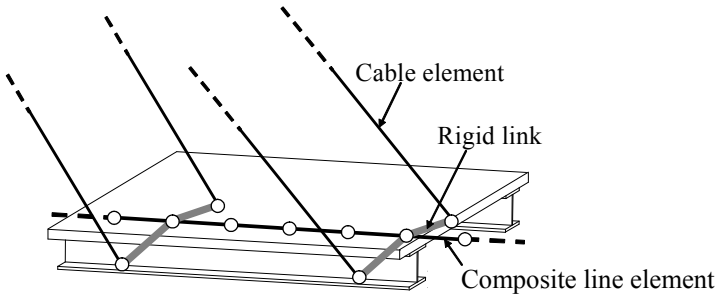

Figure 3. Combination of Composite Line Element with Rigid Links and Truss/Frame Elements

$$\boldsymbol{R_e} = \begin{bmatrix} \boldsymbol{R} & \boldsymbol{0} & \boldsymbol{0} & \boldsymbol{0} & \boldsymbol{0} & \boldsymbol{0} \\ \boldsymbol{0} & \boldsymbol{R} & \boldsymbol{0} & \boldsymbol{0} & \boldsymbol{0} & \boldsymbol{0} \\ \boldsymbol{0} & \boldsymbol{0} & \boldsymbol{I}_{22} & \boldsymbol{0} & \boldsymbol{0} & \boldsymbol{0} \\ \boldsymbol{0} & \boldsymbol{0} & \boldsymbol{0} & \boldsymbol{R} & \boldsymbol{0} & \boldsymbol{0} \\ \boldsymbol{0} & \boldsymbol{0} & \boldsymbol{0} & \boldsymbol{0} & \boldsymbol{R} & \boldsymbol{0} \\ \boldsymbol{0} & \boldsymbol{0} & \boldsymbol{0} & \boldsymbol{0} & \boldsymbol{0} & \boldsymbol{I}_{22} \end{bmatrix} \quad ; \quad \boldsymbol{R} = \begin{bmatrix} \bar{\boldsymbol{a}}_1 \cdot \boldsymbol{a}_1 & \bar{\boldsymbol{a}}_2 \cdot \boldsymbol{a}_1 & \bar{\boldsymbol{a}}_3 \cdot \boldsymbol{a}_1 \\ \bar{\boldsymbol{a}}_1 \cdot \boldsymbol{a}_2 & \bar{\boldsymbol{a}}_2 \cdot \boldsymbol{a}_2 & \bar{\boldsymbol{a}}_3 \cdot \boldsymbol{a}_2 \\ \bar{\boldsymbol{a}}_1 \cdot \boldsymbol{a}_3 & \bar{\boldsymbol{a}}_2 \cdot \boldsymbol{a}_3 & \bar{\boldsymbol{a}}_3 \cdot \boldsymbol{a}_3 \end{bmatrix} \quad ; \quad \boldsymbol{I_{22}} = \begin{bmatrix} 1 & 0 \\ 0 & 1 \end{bmatrix} \tag{4a,b,c}$$

Based on these, the nodal displacement and force vectors are transformed from the local to the global reference system based on $\bar{\boldsymbol{s}}_e = \boldsymbol{R}_e \boldsymbol{s}_e$ and $\bar{\boldsymbol{f}}_e = \boldsymbol{R}_e \boldsymbol{f}_e$. In a similar manner, also the stiffness relationship can be expressed in global coordinates using $\boldsymbol{K}_e = \boldsymbol{R}_e{}^T \overline{\boldsymbol{K}}_e \boldsymbol{R}_e$.

It is worth noting that in the cases of composite line element subjected only to flexural actions in its vertical plane, being the composite element characterised by only 10 dof, the relative 10x10 stiffness matrix needs to be expanded to dimension 16x16 by adding rows and columns of zeros to comply with the three-dimensional problem. Obviously, this results in an ill-conditioned problem solved by imposing special constraints to the element to limit rigid motions in the horizontal plane and for torsional rotations.

The freedoms of the proposed finite element are presented in Figure 2a. This element can be connected to conventional frame and truss elements using standard assembling procedures. Although different choices of nodal displacements can be used to describe the displacement field of the proposed finite element, for the selection adopted in this paper (Figure 2), the element end freedoms available for assembling to other conventional line elements (i.e. frame and truss elements) consist of the vertical deflection, rotation and axial displacement of the steel joist. The beam-slab interface slip Γ and the shear lag function ω cannot be constrained to freedoms of conventional line element and, as a consequence, no interaction can occur directly with the concrete slab. Such restriction can be easily overcome by adopting a set of independent end displacements in the formulation of the element which includes the axial displacement in the concrete component. The connectivity of the proposed element reflects common practice in which the connections among steel elements are usually preferred. For clarity, the possible connectivity used in the modelling of a cable stayed bridge is depicted in Figure 3, where the stays are connected laterally to the line element by means of rigid links.

In addition to the usual external restraints which prevent the six displacement components, other two kinds of restraints, able to prevent the interface slip and the slab warping, may be specified for the composite line element. The restraints on the slip can be used to model a deck with rigid shear connections whereas the restraint on the slab warping can simulate the presence of rigid structural elements (e.g. end transverse beams). The case of flexible transverse beams limiting the slab warping can be depicted by defining special generalized springs.

3. VALIDATION OF THE FINITE ELEMENT FORMULATION

The accuracy of the composite line element depicted in Figure 2 has been validated in the case of a realistic bridge. In the proposed application, the bridge on the Nive River built in Bayonne has been used as case study [8]. This bridge consists of a four-span continuous configuration and all relevant geometric properties are specified in Figures 4 and 5. Material properties for the steel, concrete and shear connection are: steel elastic modulus $E_s = 210$ GPa, concrete elastic modulus $E_c = 32490$ MPa, concrete Poisson's ratio $\nu = 0.15$, and shear connection stiffness $\rho = 12$ kN/mm^2. The slab is supported by cantilevered cross beams placed at a spacing of 3.78 m. The results calculated modelling the bridge with the composite line elements are compared with those obtained with a shell model (Figure 6) implemented with SAP2000 [9]. In particular, 213 line elements are used to describe the bridge deck with a total of 1703 degrees of freedoms, significantly smaller than the 53750 degrees of freedom required by the shell element model.

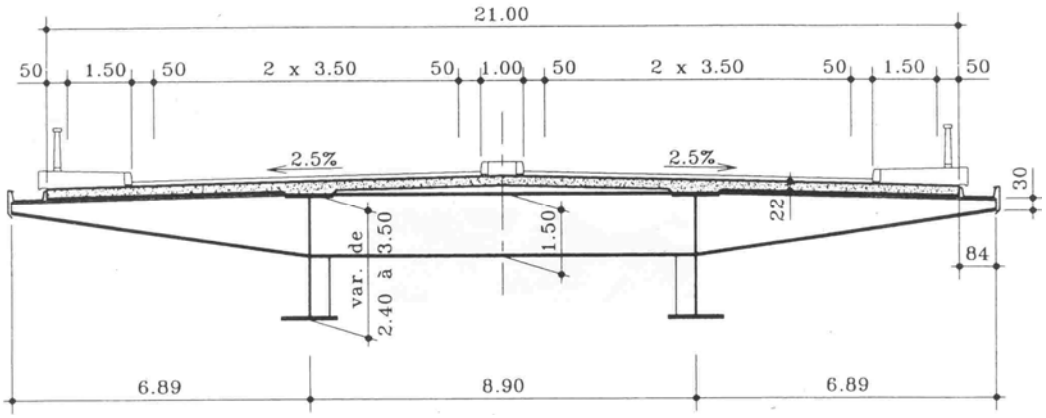

E_s = 210000 MPa
ρ = 12 kN/mm^2
E_c = 32490 MPa
ν = 0.15

Figure 4. Bridge on Nive River: Cross-section

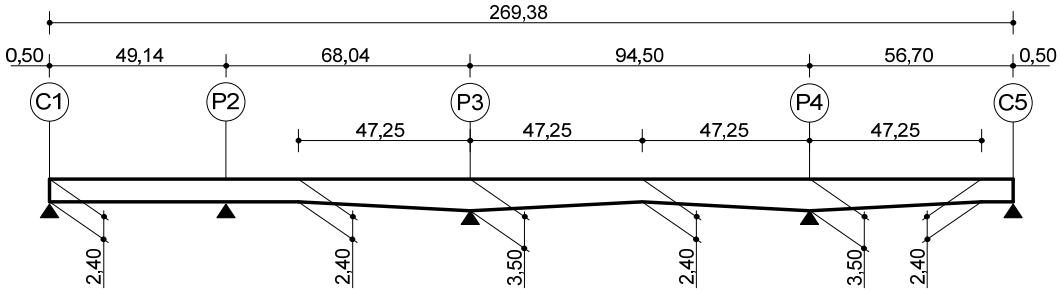

Top flange 1100 x	40	80 +20	40	80	80 +60	80	40	55	60	55	40	80	80 +60	80	40
Web	15	21	15	21			15					21			15
Bottom flange 1300 x	60	60 +35	60	80	80 +40	80	80+40				80		80 +40	80	60

Figure 5. Bridge on Nive River: Thickness of Steel Plates within the Beams

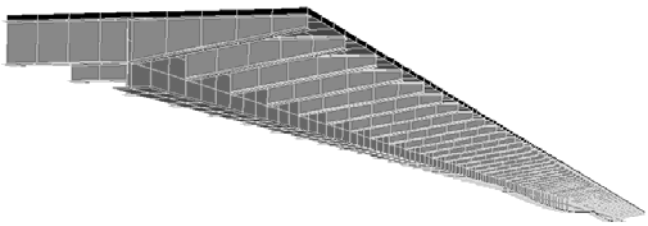

Figure 6. Bridge on Nive River: Shell Finite Element Model of the Deck

3.1 Comparisons

A vertical uniformly distributed load is applied to the top side of the slab. In the adopted numerical calculations, a line load is specified when using the line element while a surface distributed load is adopted in the shell element model. The selected case study is useful to provide insight into the influence of the cross beams, also connected to the concrete component, on the overall shear-lag behaviour of the slab.

For clarity, the results obtained using the composite line elements are reported with continuous lines while those obtained with the shell element model are illustrated with markers (circles and triangles). Figure 7 depicts the deflection and the longitudinal stresses in the bottom flange of the steel girder and Figure 8 shows the longitudinal normal stress in the middle plane of the slab for a selected set of cross-sections placed along the bridge. Based on these comparisons it is shown that the use of the composite line elements provides a very good representation of the structural response calculated with the more refined shell element model. Small discrepancies between these results occur only for the concrete slab stresses at the cross-sections 1 and 2 in Figure 8 located over and close to the end support, respectively. This is justified by the fact that, at these sections, the local transverse behaviour affects the longitudinal behaviour of the girder and the adopted model captures this localised stress diffusion only in a simplified way. Despite this, these discrepancies are not significant since at these locations the stresses are small and do not govern the design.

When considering the evaluation of the deflections, errors higher than 10% are obtained by comparing the values calculated with the proposed numerical model with those of the shell element model plotted with a dotted line with triangles (Shell a). This discrepancy was already observed in [7] for simpler bridge arrangements and was justified by the shear deformability of the steel components that is neglected in the proposed numerical formulation. The same finite element model is re-utilised for this analysis while increasing the shear modulus of the materials adopted for the shell elements. The results of this latter model have been referred to in the following as 'Shell b' to distinguish them from those calculated using the initial FE model denoted as 'Shell a'. The discrepancies observed for the deflection using model 'Shell a' become negligible when using model 'Shell b' as shown with the dotted line and circular marks in Figure 7, in which case the latter line becomes coincident with the continuous curve representing the proposed numerical model. It is worth noting that this change in the shear modulus also affects the discrepancy of the concrete stress states at cross-section 4 (Figure 8), becoming less remarkable as the shear deformability of the beam becomes negligible.

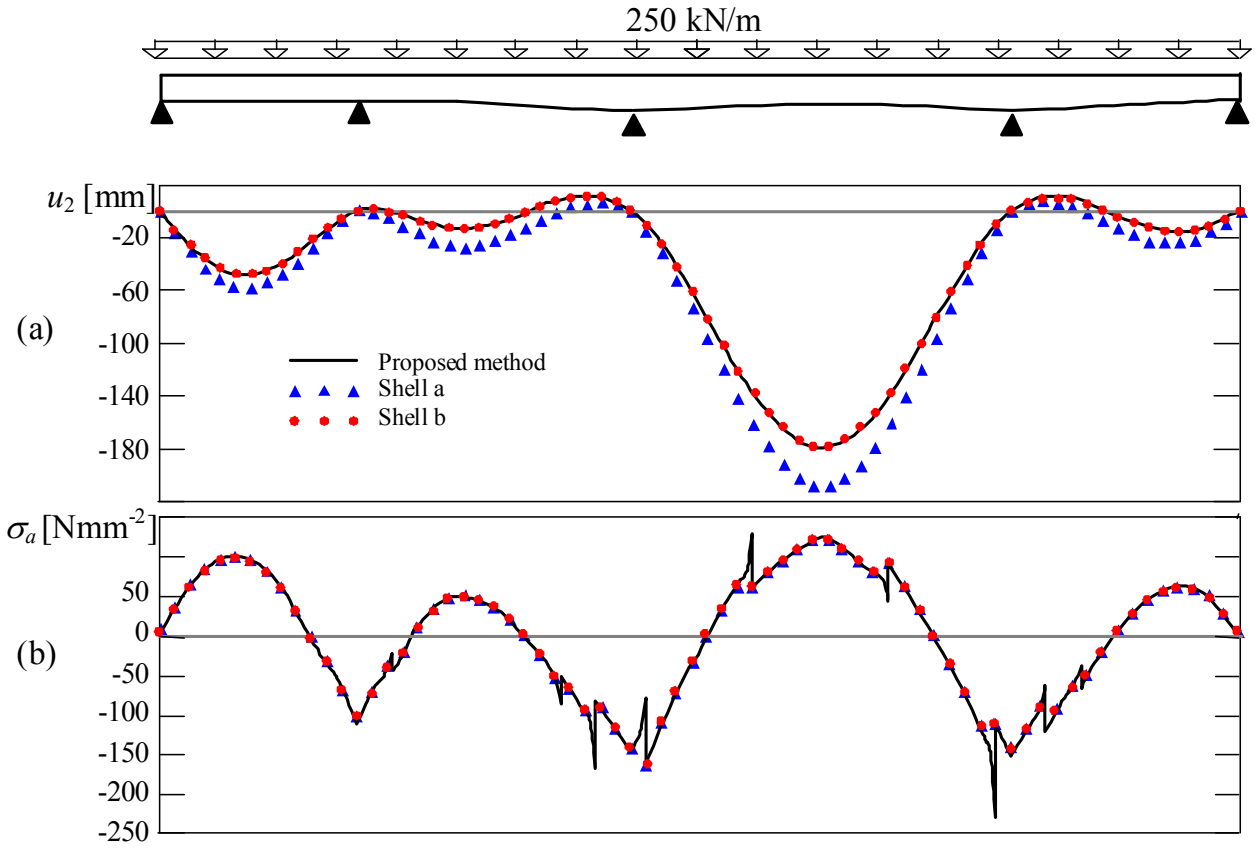

Figure 7. Bridge on Nive River:
(a) Deflection of the Deck (b) Longitudinal Stresses in the Bottom Flange of the Steel Girders

In regards to the occurrence of shear-lag effects, the presence of cross beams does not affect the overall response. This is partially due to the fact that cross beams do not constitute a restraint against the slab warping because of their low lateral and torsional stiffness. As the concrete stresses are evaluated at the mid-height of the slab, these are only affected by the membrane action of the slab and not by its bending one that is more influenced by the presence of the cross-beams.

Of course this is a limit of the proposed model that nevertheless maintains its validity in describing the behaviour of the bridge and confirms to be a good tool for the verification of the composite cross-sections. It is worth noting that, if necessary, bending effects of the slab may be easily evaluated with partial models (or also with available charts) and superimposed to the membrane effects to evaluate the maximum stresses at the top or bottom plane of the slab.

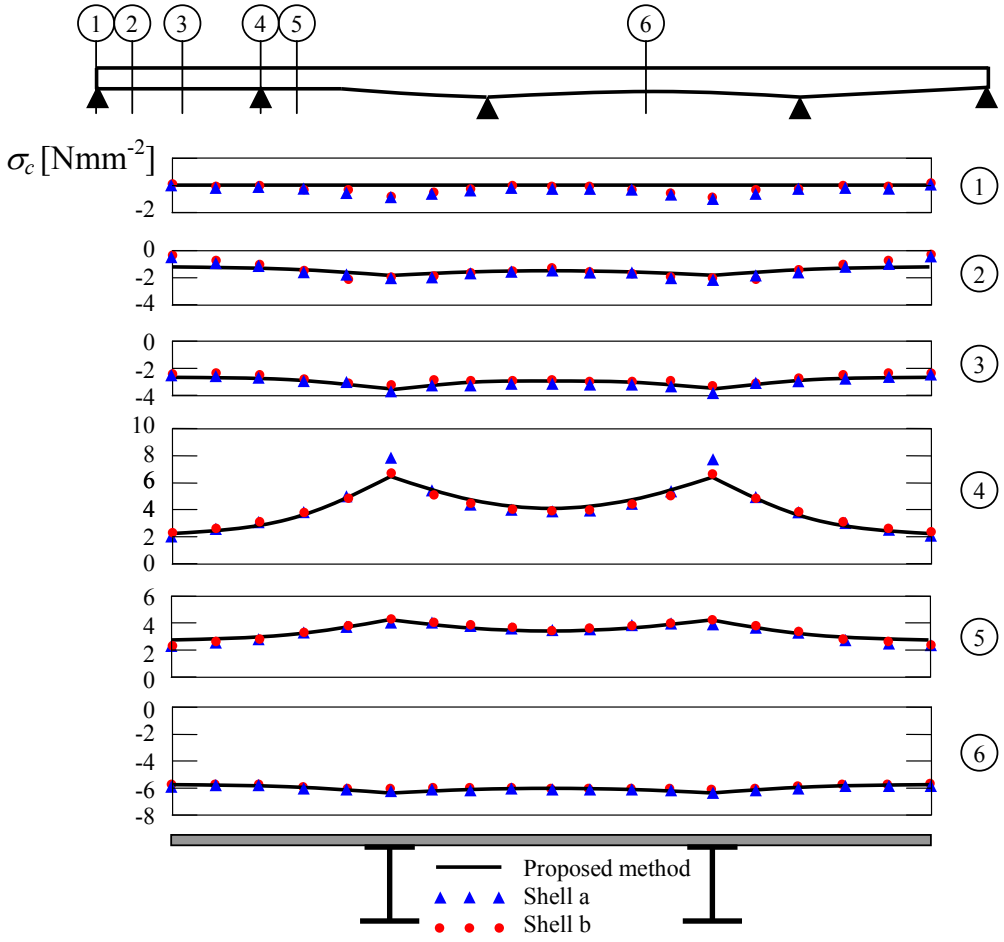

Figure 8. Bridge on Nive River: Longitudinal Stresses in the Middle Plane of the Slab

4. APPLICATION TO A CABLE STAYED BRIDGE

A cable-stayed bridge is considered to outline the capabilities of the proposed composite finite element, when combined with other truss and frame elements, to model complex bridge systems. The case study considered is shown in Figure 9. This consists of a steel-concrete composite deck supported by two reinforced concrete pylons, higher than 70 m, and by 28 couples of stays pretensioned to control the deck deflection and the horizontal displacements of the pylons. Two anchor piers are placed at the bridge ends. The reinforced concrete slab of the deck is 0.23 m thick and is sustained by cross beams supported by the two longitudinal main girders. The spacing between

stays' anchorages is 18 m. The cylinder strength of the concrete used for the slab and the pylons is $f_{ck} = 45$ N/mm^2; the elastic constants $E_s = 165000$ N/mm^2 and $E_a = 210000$ N/mm^2 are considered for the stays and the structural steel, respectively.

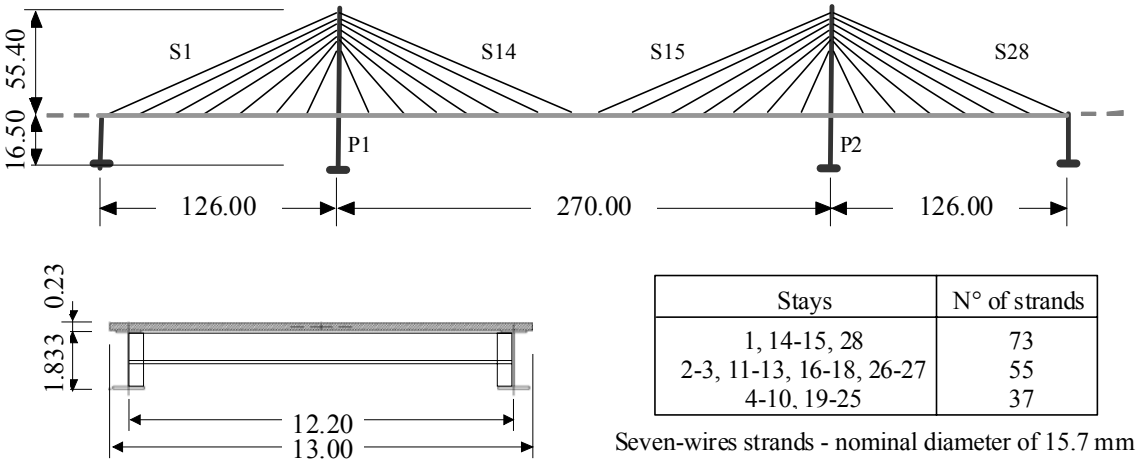

Stays	N° of strands
1, 14-15, 28	73
2-3, 11-13, 16-18, 26-27	55
4-10, 19-25	37

Seven-wires strands - nominal diameter of 15.7 mm

Figure 9. General Layout and Dimensions of the Cable-stayed Bridge Considered

The proposed finite element is used for the composite deck whereas common truss and beam elements are used for the stays and the pylons, respectively; in order to ensure the correct positioning of the stays at the sides of the bridge, rigid links have also been used in the model.

Short- and long-term analyses are carried out considering the following loading conditions: (i) a uniformly distributed load (UDL) of 150 kN/m, representing the self-weight and other permanent loads; (ii) UDL and shrinkage; and (iii) traffic loads (TL) applied at the central span.

The long-term analyses are carried out by means of the Effective Modulus Method as recommended in [1]. With this approach an effective elastic modulus $E_{eff}(t,t_0)$ is adopted for the concrete when considering the time-dependent behaviour which is calculated as:

$$E_{eff}(t,t_0) = \frac{E_c(t_0)}{1+\psi_L \phi(t,t_0)} \tag{5}$$

in which $E_c(t_0)$ is the concrete elastic modulus calculated at the time of first loading t_0, $\phi(t,t_0)$ depicts the creep coefficient defining the creep occurred at time t for a stress first applied at time t_0, and ψ_L represents the creep multiplier which depends on the type of loading and its values are based on European guidelines [1]. In particular, the value for ψ_L used for sustained loads and prestressing of stays is 1.1. The effects of concrete shrinkage are evaluated using a ψ_L value of 0.55 and a creep coefficient $\phi(t,t_s)$ defined with respect to time t_s, which is the instant at which shrinkage is supposed to start (end curing). The creep coefficients and the shrinkage action are defined according to Eurocode 2 [10].

Results are presented in terms of deflections, stress state in the steel beams and concrete slab and effective width of the slab. Figure 10 shows the results obtained considering both short- and long-term actions calculated at 28 and 20000 days, respectively. In particular, the results of the short-term analysis carried out are reported along the whole bridge whereas long-term results are reported with and without shrinkage action in the left and right sides of the diagrams, respectively.
The deck deflection is depicted in Figure 10a. The short-term results are characterised by null displacements at the stays anchorage as a consequence of the prestressing. Long-term deflections

slightly increase as creep and shrinkage develop. It is worth noting that the configuration of zero-deflection, achieved in the instantaneous analysis balancing the self-weight of the deck by means of the stays' prestressing, is lost in the long-term even if the modifications are not important since they are within 80 mm.

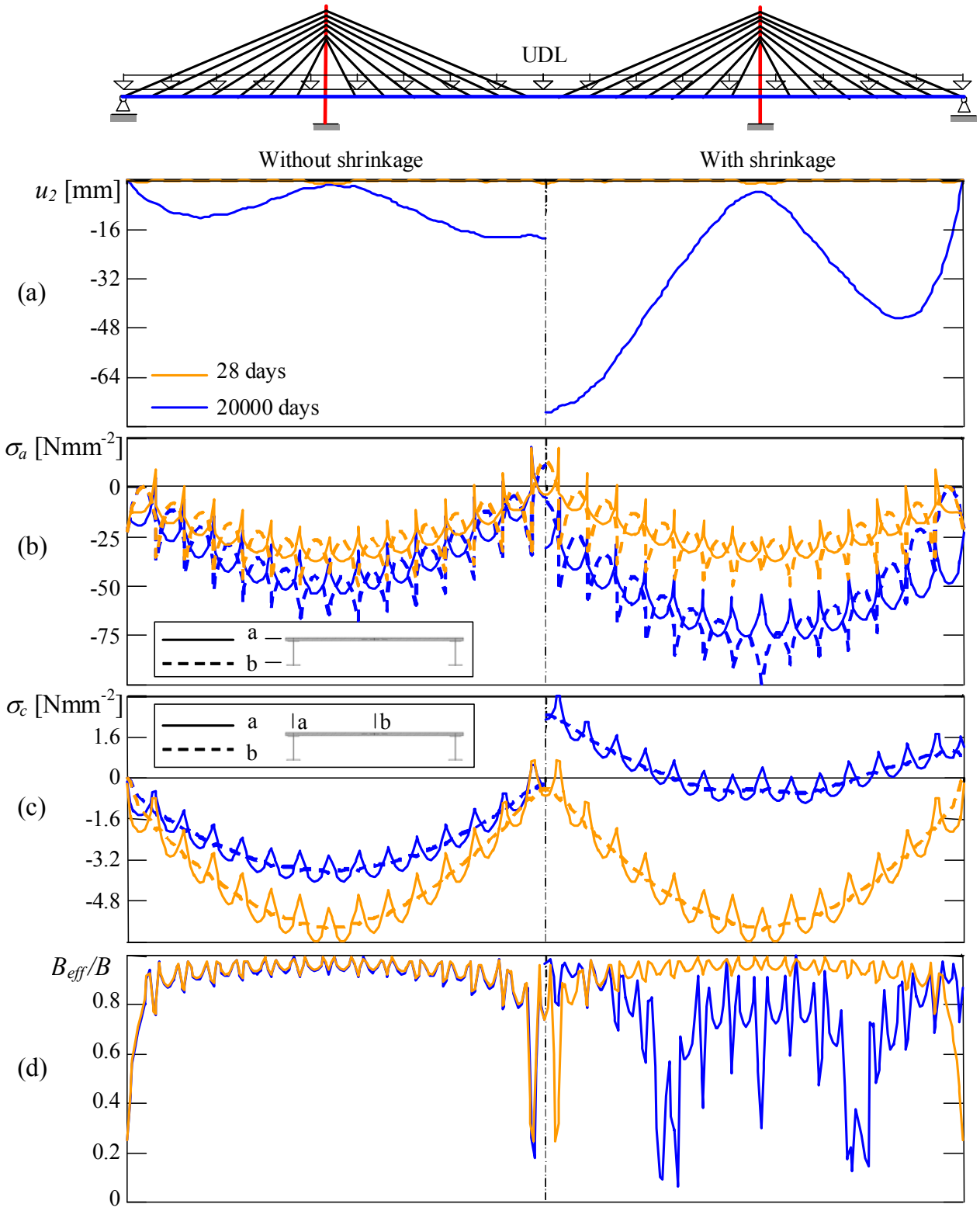

Figure 10. Permanent Actions: (a) Deck Deflection; (b) Longitudinal Normal Stresses in the Top and Bottom Flanges of the Steel Beam; (c) Longitudinal Normal Stresses at Mid-height of the Slab; (d) Effective Width over the Actual Deck Width

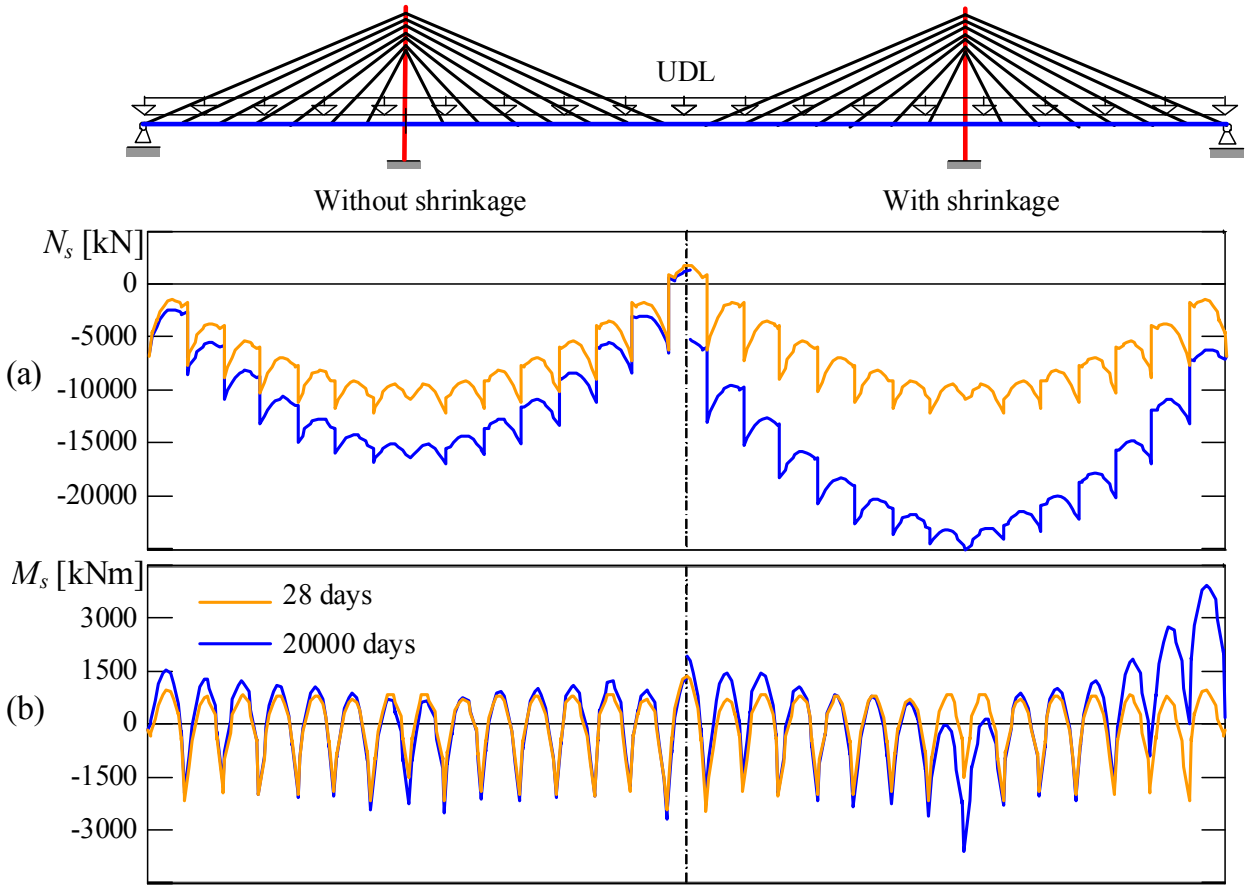

Figure 11. Permanent Actions: (a) Axial Force and (b) Bending Moment of the Steel Beam

The stresses obtained for the top and bottom steel flanges are illustrated in Figure 10b while Figure 10c plots the stresses calculated at mid-height of the slab along the bridge length at the location of the steel member axis and along the centre-line of the deck. The slab effective width is determined based on the calculated stress distributions and is illustrated in Figure 10d.

The stress distributions in the steel girders (Figure 10b) are determined based on the axial force that, as expected, is maximum near the pylons and minimum at the deck ends and at mid-span of the central span (Figure 11a), and on the bending moment that varies between each couple of stays according to parabolic curves (Figure 11b). Due to the long-term behaviour of the concrete, the compressive axial forces grow in time. In particular, the effect of shrinkage is quite remarkable as shown in the right side diagram of Figures 10b and 11a.

Near the longitudinal steel members the concrete stress distribution has a distinguished varying pattern which tends to smoothen when moving towards the centre-line of the cross-section (Figure 10c). This demonstrates the effects produced by the concentrated forces exerted by the stays' anchorages. The diffusion mechanism captured by the model is such that for cross-sections close to the stay anchorage, the higher stress value are obtained along the longitudinal beams while for cross-sections placed between two consecutive stay anchorages, the stress maximum value is obtained at the centre-line of the slab. When considering long-term effects, the concrete compressive stresses tend to reduce with time; in particular, the effects of shrinkage produces tensile stresses for large deck sections where prestressing due to stays becomes less significant. This is particularly evident from the contour diagrams of the slab that highlight sections characterised by peaks of tensile stresses for the slab sections in the proximity of stays' anchorages (Figure 12).

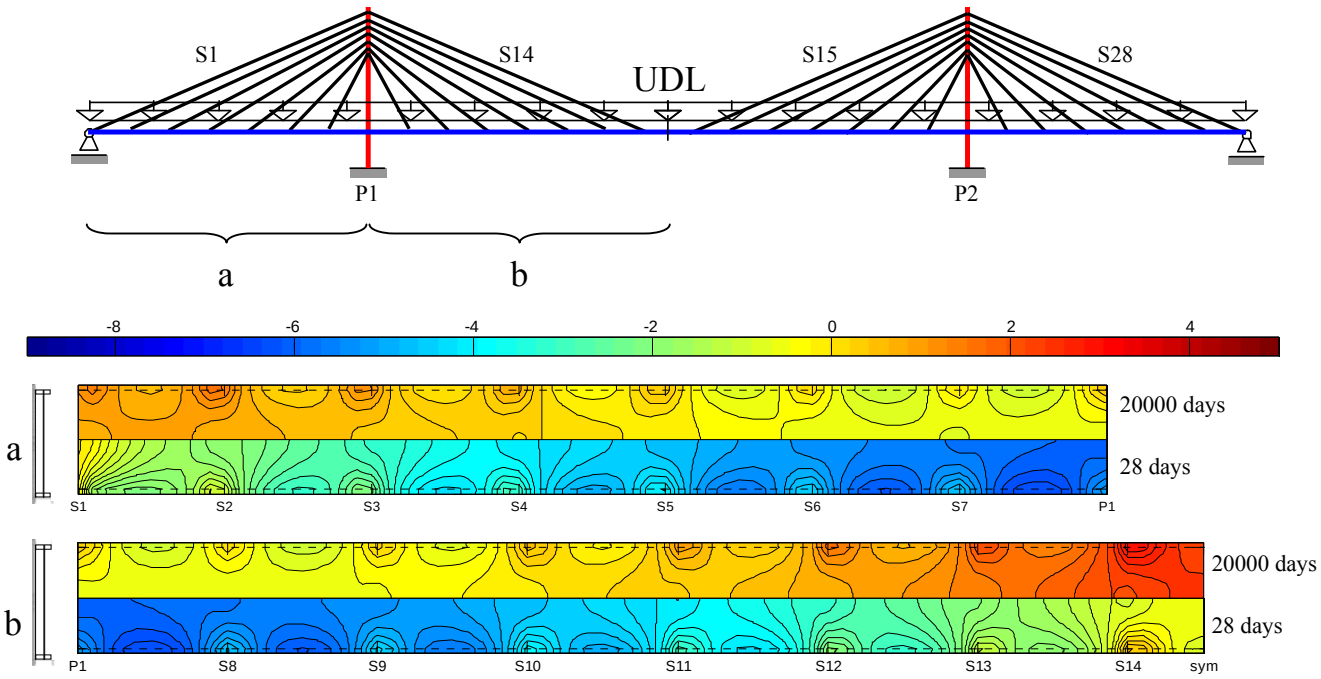

Figure 12. Permanent Actions: Contour Plots of Stresses in the Reinforced Concrete Slab due to Permanent Actions

Particular attention is required when analysing the results in Figure 10d where the slab effective width is plotted. In the short term, it may be observed that the fluctuation reflects the variation of the compressive stresses in the slab and that, excepting for slab sections at the middle of the central span and at the bridge ends, the effective width remains within 0.9 and 1.0 times the real slab width; the very low values obtained for the other sections previously mentioned (less than 0.4) are due to the fluctuation of stress compared with the low overall compression of the slab. It is worth highlighting that the localised minimum values observed are not relevant from a design viewpoint as related to bridge segments along which the stress levels are relatively low.

The long-term effects on the definition of the slab effective width are strongly characterised by the concrete shrinkage; this produces a significant reduction of the effective width (down to 0.7) also for sections characterised in the short-term analyses by moderate effects of stress concentrations. This is due to shrinkage which is responsible for inducing tensile stresses, almost uniformly distributed within the whole slab except for the end sections, that superimpose onto stresses due to permanent loads and stays' pretensioning. In this process shrinkage does not modify the fluctuation at the lateral beam locations but mainly reduces the overall axial force in the slab by magnifying the stress concentration.

Table 1 shows the effects of the different load cases considered on the stays' pretensioning forces. It is evident that the long-term effects are such that only small variations of the internal forces are induced in the stays.

Table 1. Axial Forces in the Stays due to Prestressing and Permanent Actions

Stays	28 days	20000 days Without shrinkage		20000 days With shrinkage	
	[kN]	[kN]	(%)	[kN]	(%)
1, 28	3800	3729	(-1.9)	3559	(-6.3)
2, 27	3333	3310	(-0.7)	3314	(-0.6)
3, 26	2869	2871	(+0.1)	2943	(+2.6)
4, 25	2589	2601	(+0.5)	2658	(+2.7)
5, 24	2225	2240	(+0.7)	2281	(+2.5)
6, 23	1805	1812	(+0.4)	1809	(+0.2)
7, 22	1570	1540	(-1.9)	1427	(-9.1)
8, 21	1570	1548	(-1.4)	1456	(-7.3)
9, 20	1804	1812	(+0.4)	1804	(0.0)
10, 19	2230	2242	(+0.5)	2254	(+1.1)
11, 18	2569	2579	(+0.4)	2600	(+1.2)
12, 17	2947	2943	(-0.2)	2958	(+0.4)
13, 16	3085	3061	(-0.8)	3057	(-0.9)
14, 15	3975	3917	(-1.5)	3864	(-2.8)

Figure 13 shows the results obtained by considering traffic loads at the central span. According to the Load Model 1 of Eurocode 1-2 [11], four notional lanes are considered within the deck width; this results in a uniformly distributed load of 52 kN/m and in a couple of concentrated loads of 700 kN. On the left side of the diagrams, the results are superimposed on the short-term stresses due to permanent loads whereas on the right side the same are superimposed on long-term stresses inclusive of shrinkage. Also in this case it is interesting to highlight the differences between the short- and long-term behaviours, which are strongly characterised by shrinkage, and how the effective width is sensitive to the loading conditions. Figure 14 shows a contour plot of stresses at mid-height of the concrete slab.

5. CONCLUSIONS

This paper presented an implementation for design applications of a composite line finite element based on partial interaction theory. The element is suited for capturing the shear-lag effects and its use is suitable for composite steel-concrete decks for which the assumption of preservation of the plane cross-section is not valid due to the large widths of the slabs when compared to their thickness. Models of complex bridges may be easily developed without considerations of the definition of the effective cross-section when combining the use of this element with other line elements (trusses and frame beams).

The proposed formulation is able to account for shear-lag effects in complex bridges where simplified methods are not applicable. Based on this formulation, the effective widths to be used in design are calculated consistently for each load combination and the produced results can be used by a designer following standard procedures.

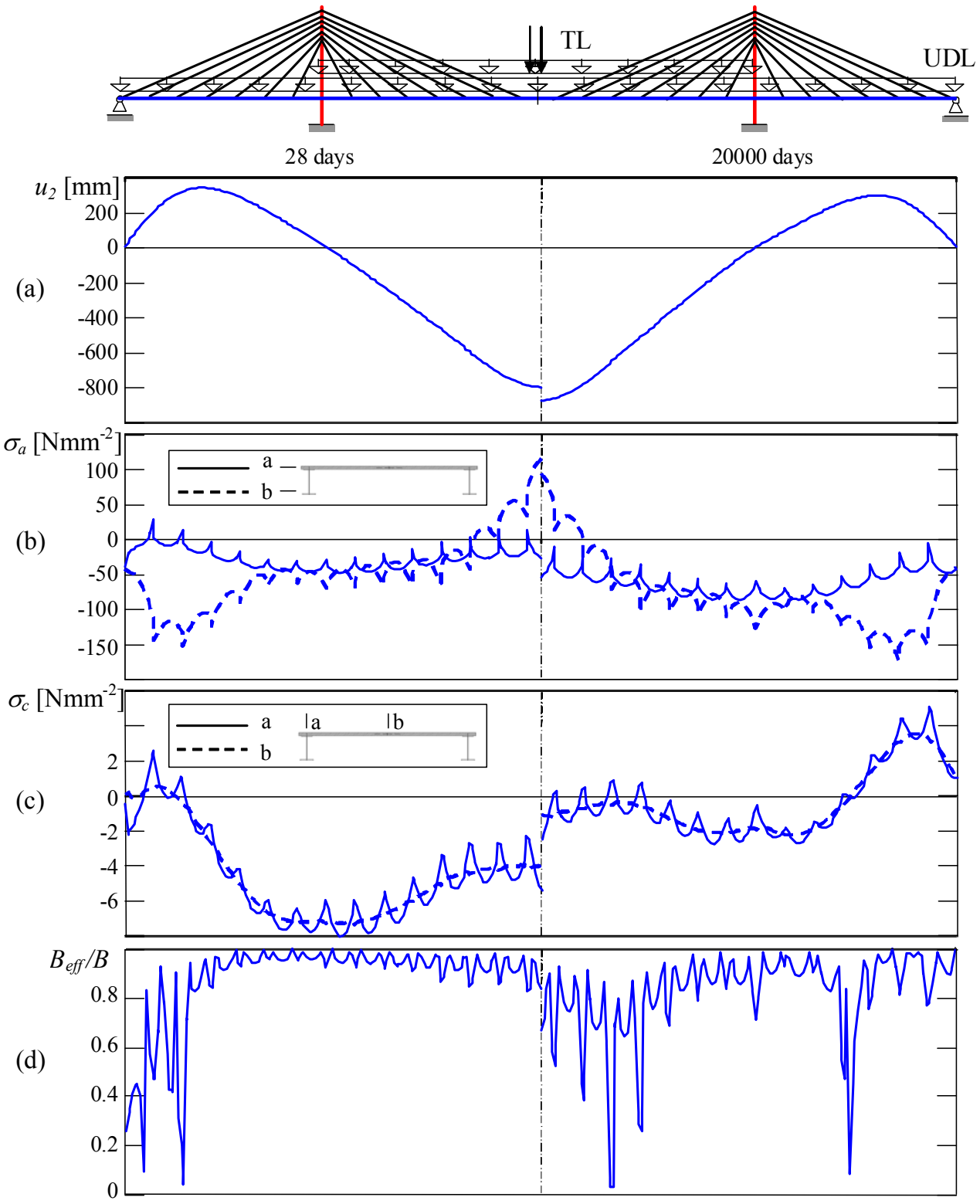

Figure 13. Traffic Loads: (a) Deck Deflection; (b) Longitudinal Normal Stresses in the Top and Bottom Flanges of the Steel Beam; (c) Longitudinal Normal Stresses at Mid-height of the Slab; (d) Effective Width over the Actual Deck Width

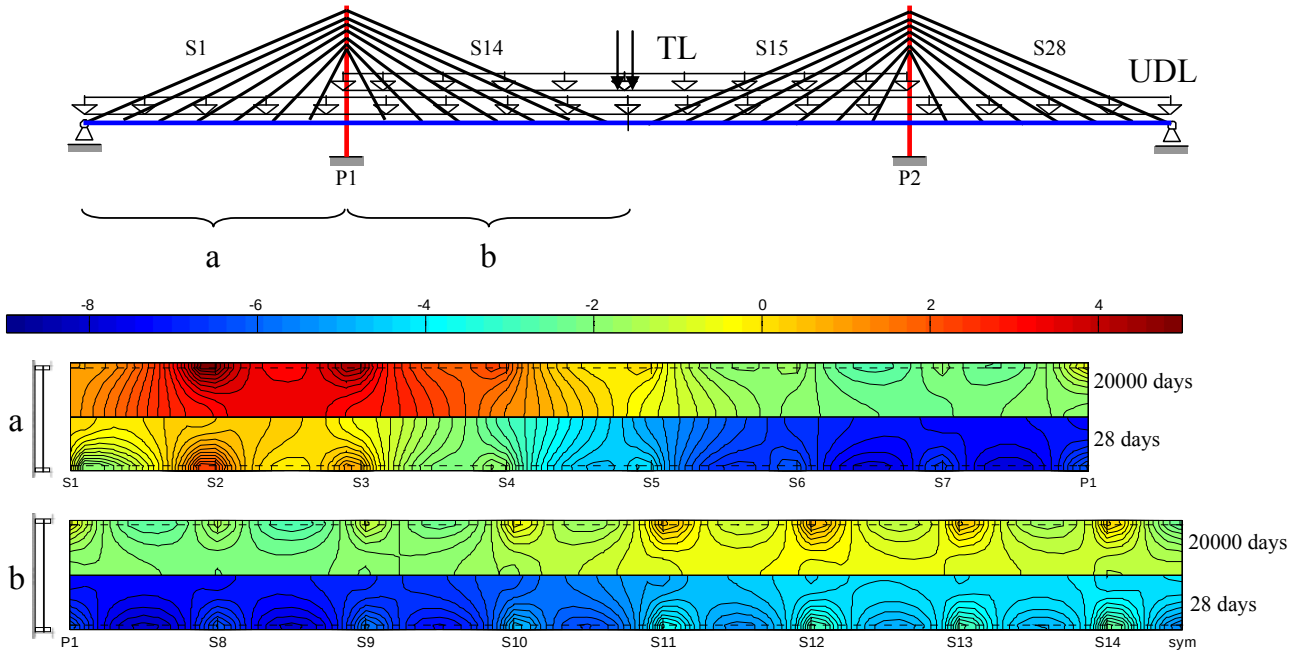

Figure 14. Traffic Loads: Contour Plots of Stresses in the Reinforced Concrete Slab due to Permanent Actions

With respect to refined finite element models (e.g. using shell elements) the method has the advantage of reducing the amount of degrees of freedom without loss of precision in evaluating stress states. The precision of the method was demonstrated by applying the use of the deck finite element to a real bridge and comparing the results with those given by refined shell finite elements. The proposed method produces very good results for what concern stresses in the steel beams and in the concrete slab while a lower level of precision is obtained in the evaluation of deflections due to the shear strains of the steel beams that are neglected in the model. The presence of cross beams, even if connected to the reinforced concrete slab, does not affect the results.

A cable stayed bridge subjected to different actions (permanent loads, shrinkage and traffic loads) has then been considered and analysed. Both short- and long-term analyses were carried out to demonstrate the importance of long-term effects and the difficulties that a designer could have in choosing adequate slab effective widths as these depend sensibly on the loading layouts and are time dependent.

The limitation of the proposed formulation relies on its inability to account for torsion and transverse bending but the authors do not feel that this compromises the usefulness of the proposed element which intends to complement the analysis tools available to bridge designers.

ACKNOWLEDGEMENT

The work carried out in this article by the second author was supported by a Discovery Project awarded under the Australian Research Council's funding scheme and through a research grant awarded by the Commonwealth through the Australia-Korea Foundation of the Department of Foreign Affairs and Trade.

REFERENCES

[1] EN 1994-2, "EUROCODE 4: Design of Composite Steel and Concrete Structures - Part 2: General Rules and Rules for Bridges", European Committee for Standardization, 2005.

[2] Dezi, L., Gara, F., and Leoni, G., "Effective Slab Width in Prestressed Twin-girder Composite Decks", Journal of Structural Engineering, ASCE, 2006, Vol. 132, No. 9, pp. 1358–1370.

[3] Gara, F., Ranzi, G. and Leoni, G., "Analysis of the Shear Lag Effect in Composite Bridges with Complex Static Scheme by Means of a Deck Finite Element," International Journal of Steel Structures, 2008, Vol. 8, pp. 249-260.

[4] Reissner, E., "Analysis of Shear Lag in Box Beams by the Principle of the Minimum Potential Energy", Quarterly of Applied Mathematichs, 1946, Vol. 4, No. 3, pp. 268–278.

[5] Dezi, L., Gara, F., Leoni, G. and Tarantino, A.M., "Time Dependent Analysis of Shear-lag Effect in Composite Beams", Journal of Engineering Mechanics, 2001, Vol. 127, No. 1, pp. 71-79.

[6] Dezi, L., Gara, F. and Leoni, G., "Shear-lag Effect in Twin-girder Composite Decks", Steel and Composite Structures, 2003, Vol. 3, No. 2, pp. 111–122.

[7] Gara, F., Leoni, G. and Dezi, L., "A Beam Finite Element Including Shear Lag Effect for the Time-dependent Analysis of Steel-concrete Composite Decks", Engineering Structures, 2009, Vol. 31, pp. 1888–1902.

[8] Kretz, T., Michotey, J. and Svetchine, M., "5ème pont sur la Nive", Bulletin Ponts Metalliques, SETRA, 1992, Vol. 15, pp. 133-136. (in French)

[9] SAP2000, "Computer and Structures, Inc. CSI Analysis Reference Manual", Berkeley, California, 2004.

[10] EN 1992-1-1, "EUROCODE 2: Design of Concrete Structures - Part 1-1: General Rules and Rules for Buildings", European Committee for Standardization, 2004.

[11] EN 1991-2, "EUROCODE 1: Action on Structures - Part 2: Traffic Loads on Bridges", European Committee for Standardization, 2003.